Proceedings of
2001 ASME International Mechanical Engineering Congress and Exposition
November 11-16, 2001, New York, NY

OMNIDIRECTIONAL WALKING MICROROBOT REALIZED BY THERMAL MICROACTUATOR ARRAYS

Matthew H. Mohebbi, Mason L. Terry, Karl F. Böhringer
Department of Electrical Engineering
University of Washington

Gregory T. A. Kovacs
Department of Electrical Engineering
Stanford University

John W. Suh
Systems and Practices Laboratory
Xerox Palo Alto Research Center

ABSTRACT

An omnidirectional mobile microrobot realized by microelectromechanical system (MEMS) actuator arrays is presented. The microrobot consists of two rigidly connected microcilia array chips, each having an 8×8 array of "motion pixels," which are composed of four orthogonally oriented thermal bimorph actuators. This allows for reliable, accurate motion in three degrees of freedom (x, y, θ) in the plane, a first for a microrobot of this kind. The microrobot is approximately 3cm in length, 1cm in width, 1mm in height, and has a mass of less than half a gram. By varying the input power, actuation frequency and motion gait strategy the velocity of the chip can be precisely controlled. Motion in three degrees of freedom has been demonstrated and a maximum velocity of 635 μm/s and carrying capacity greater than 1.448 g (two 8-pin ICs) has been observed. The microrobot has been characterized extensively and a model for its performance is described.

Keywords: Walking chip, microrobot, omnidirectional, actuator array, micromanipulation, bimorph, polyimide

INTRODUCTION

Mobile microrobots have been envisioned for a wide variety of applications, including security and surveillance, health care, space exploration, hazardous environment monitoring, manufacturing and others. Few microrobots, however, have been developed utilizing MEMS technology, partly due to the difficulty in coupling the microsystems to the macroworld. Issues such as structural strength, specifically in the actuators, range of actuator motion, and power delivery must be addressed for these microrobots to become useful devices. The advantages of MEMS based micromachined robots include batch-fabrication with the possibility of integrated on-chip circuits, microfuel cells and various microsensors.

In this paper, we present the first MEMS based microrobot that has been extensively characterized for reliable and repeatable motion in all 3 degrees of freedom (DOF) in the plane. First, some related work is shown for both microconveyors and some previous microrobot designs. Next is an introduction to the key MEMS technology, the experimental setup and microrobot operation including experimental conditions. Following are the experimental results summed up by a discussion and conclusions.

Related Work

There have been many small robots assembled from *conventionally* machined components, some smaller than 1cm^3. In this paper, however, we focus on *MEMS* based systems.

While MEMS based mobile microrobots have been scarce thus far, good progress has been made in recent years in micro conveyor systems, whose goal is to precisely transport and position tiny objects with distributed micro manipulators.

Micro conveyors. Many microactuators are, by their very nature, weak individually both in output force and damage susceptibility. Micromanipulator arrays address these issues by utilizing a large number of actuators in parallel and thus distributing the load. By using specific gait patterns, these actuators work in concert to move an object similar to the way in which a crowd moves a crowd-surfer [1, 2, 3, 4, 5, 6].

Many methods of actuation have been investigated ranging from air jets [7, 8, 9], electromagnetic actuators [10, 11, 12], piezoelectric actuators [13], electrostatic actuators [14], thermal-bimorph actuators [15, 16, 17, 18, 19] and electrothermal actuators [20, 21].

In principle, most of these systems could be transformed into moving microchip robots by simply flipping them over and operating them upside-down. In actuality, problems such as power delivery, self-supporting strength and heat dissipation arise, making implementation difficult in practice.

Walking microrobots. Previous MEMS-based microrobots have been demonstrated by several different groups. Three designs are are briefly described below.

Ebefors et al., using polyimide v-groove joints with 1-DOF [22], created a microrobot capable of carrying loads of more than 30 times the weight of the robot at a velocity of 4 mm/s, and power of 1.08W. The maximum velocity reached is 6 mm/s [23]. The dimension of the design, including leg length, is $15 \times 5 \times 1.5$ mm.

Kladitis et al., using thermal actuated, manually erected silicon legs in a MUMPs design, realized two microrobot prototypes [21], the first with 96 legs and 2-DOF, the second with 90 legs and 1-DOF. No locomotion could be demonstrated, possibly due to the attachment wire mass and stiffness although both were shown effective as microconveyors. The 2-DOF prototype transports a mass of 3.06 mg at 7.55 μm/s with a drive frequency of 2 Hz. The dimension of the prototypes is $10 \times 10 \times 0.75$ mm.

Yeh et al. fabricated an exoskeleton for a microrobot [24]. This exoskeleton has 6 2-DOF legs which are proposed to be electrostatically actuated (not yet implemented). Dimensions given for the robot exoskeleton are 5×10 mm.

FABRICATION

The robot in this paper is based on the thermal bimorph microcilia originally described by Suh et al. [17]. These microactuators have been used in a variety of micropositioning applications including scanning electron microscope stages [25] and microspacecraft docking [26].

The cilia actuators consist of a titanium tungsten (TiW) resistor heater loop sandwiched between two thin-film polyimide layers with different coefficients of thermal expansion (CTE). The bottom polyimide has a low CTE whereas the top layer has a high CTE. The curing temperature of 350 °C causes thermal strain between the two polyimide layers when they cool down to room temperature. Once released from the substrate the actuator curls out of the plane. The vertical and horizontal deflection of the actuator tip average 130μm and 30μm respectively. When current is passed through the TiW resistor heat is transferred to the polyimide layers. The heat reduces the strain in the actuator causing it to curl towards the substrate. With an applied voltage of 7.5V per actuator the vertical tip height reduces by approximately 30μm.

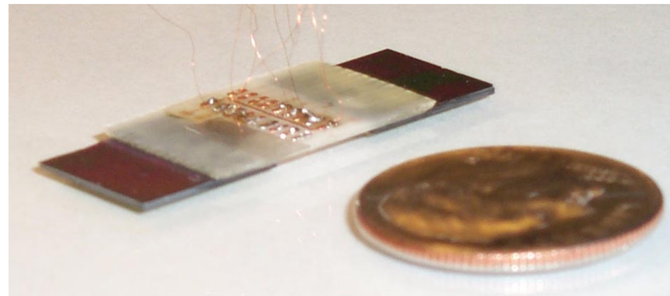

Figure 1. Microrobot in relation to a US Dime. Note the two dark green (grey) cilia chips bonded to the white PCB board. Wire bonds on the bottom side connect the 5 channels of each chip to pads on the PCB board. Nine wires (two sets of four directions plus a common ground) soldered to the top side pads connect the robot to the control box.

An actuator chip (1cm $\times$ 1cm) is composed of 256 cilia in an 8×8 array of cilia motion pixels where each motion pixel contains four orthogonally oriented cilia actuators. The four actuators of the motion pixels are independently controlled by four channels, labeled by their directional orientation (North, South, East, West).

EXPERIMENTAL SETUP

The microrobot is constructed using two of the cilia chips and a printed circuit board (PCB). Using two chips provides increased stability over a single chip design and allows for motion in the θ direction. The chips were bonded to a PCB backbone. Wire bonds connect the five channels of each chip to the PCB. Using a common ground on the PCB, nine 25μm insulated copper wires (California Fine Wire - Cu 99.99%, CDA 101, H-Poly Red) connect the chip to the controller. An image of the microrobot is shown in Figure 1. The mass of the microrobot is 0.457g with a volume of $30 \times 10 \times 1$ mm.

The controller consists of custom circuitry and a LabView interface running on a PC. The LabView interface allows the selection of individual chip directional control (8 directions), desired gait (two-, three-, or four-phase), and control signal frequency. Cilia states may change at the rising and falling edge of the control signal. A 10×10 cm glass plate is used for the interface surface that the microrobot walks upon.

For data collection, a tracking pattern consisting of two high resolution circles 100 μm in diameter and spaced 500 μm apart is placed on the PCB board and video of the robot's motion is digitally captured with a video microscope. The frames of the movie are then imported into Matlab and smoothed using a gaussian kernel. A 2D convolution is then performed on the entire first frame to establish the tracking circles' initial locations and an incremental neighborhood tracking method is employed for the remaining frames.

Modeling and Data Fitting

We hypothesize that the motion of the microrobot is governed by the following equation:

$$f(t) = at + b(1 - e^{-ct}) \tag{1}$$

This equation consists of a linear term $at + b$ and an exponentially decaying term $-be^{-ct}$), which models the decrease of cilia motion range with increasing operating temperature. Note that $f(0) = 0$. The parameters $a, b, c \geq 0$ depend on the specific properties of the cilia and operation conditions including input power, heat dissipation, and interfacial surface properties.

With Equation 1 we can calculate the velocity of the microrobot as follows.

$$f'(t) = a + bce^{-ct} \tag{2}$$

In particular, the instantaneous velocity at start of operation is $v_0 = f'(0) = a + bc$, and the asymptotic velocity for $t \to \infty$ is $v_\infty = f'(t \to \infty) = a$. The time constant τ that relates the heating of the cilia chips to the robot's velocity is given by $\tau = -c$.

Using a Monte Carlo search method, the best fit for the experimental data to equation 1 is determined by iteratively generating values for parameters a, b, c to minimize the least squares fit.

OPERATION

By actuating opposing cilia in specific sequences a three- and four-phase walking gait can be achieved. The four-phase gait consists of actuating opposing cilia in the sequence: start with both north and south relaxed, north actuated, south actuated, north relaxed, south relaxed, repeat. This sequence would move the robot in the south direction. A three-phase gait is realized in the following sequence: both north and south relaxed, north actuated, south actuated at the same time that north is relaxed, south relaxed. This sequence would also move the robot in the south direction. For an actuation voltage of 7.5V a step size of 5 μm is seen where two steps complete one four-phase gait cycle. Additionally, lower voltages allow smaller step sizes providing highly accurate positioning.

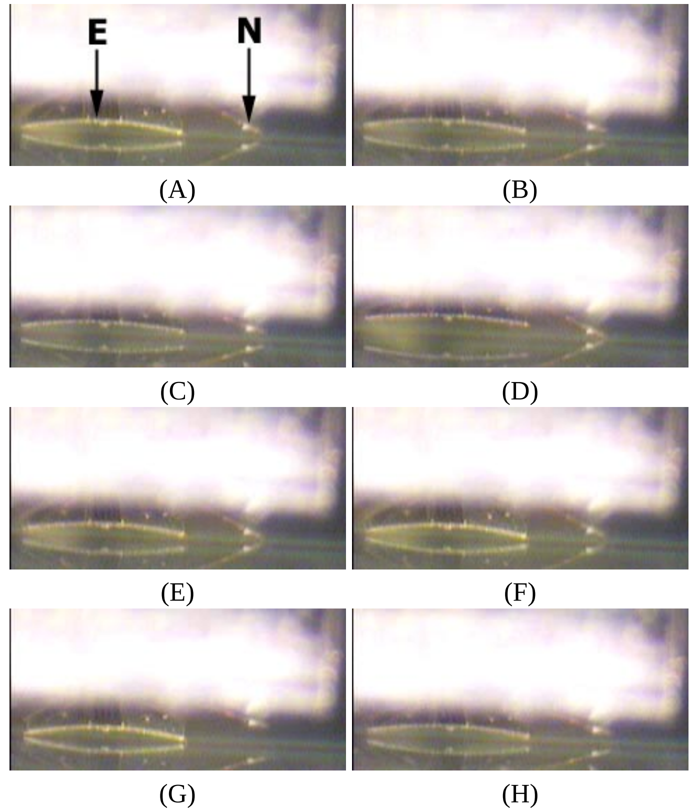

Figure 2. Video frames of a single motion pixel during northwest movement at 10Hz. Note from this view point, the east actuator is seen head on and only the contour of the north actuator is visible. A) At the beginning of the gait cycle the north and east actuators are unpowered (curled out of plane). B & C) A drive of 60V is applied to the east channel causing it to curl towards the substrate, while the west channel is left unpowered. D) The drive is sustained on the east channel and is applied to the west, causing the chip to fall westward. E) The drive is turned off on the east channel, pushing the chip westward. 60V is applied to the south channel. F) The east actuator returns to the normal out of plane position while a drive is applied to the north actuator, causing the chip to fall northward. G) The drive is sustained on the north channel and removed from the south, pushing the chip northward. H) The drive is removed from the north channel and the north actuator returns to its normal position. The gait cycle is then repeated.

Gaits for eight motion directions (along the axis and along diagonals, Figure 2) have been implemented for the individual chips. By actuating the front and back chips in the east and west directions respectively, rotation of the microrobot is achieved. Rotation can also be realized by actuating the front and back

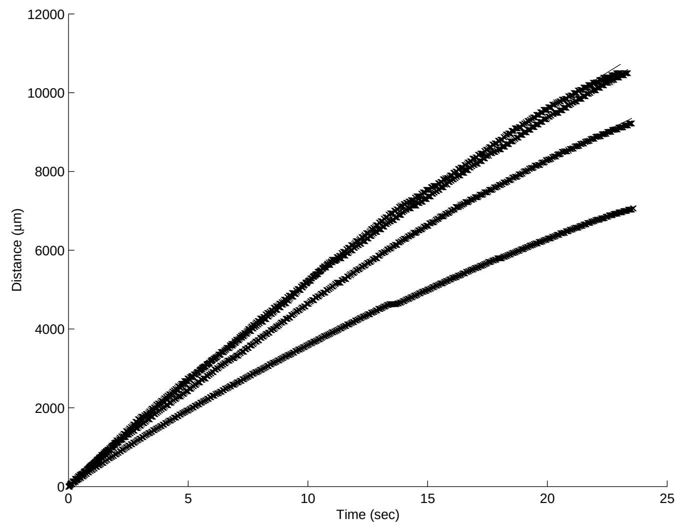

Figure 3. Northwest motion translational displacements, plotted as “x”, and the best fit curve. Plots represent, from bottom up, 30, 60, 120 and 90Hz control frequencies. The highest velocity for these frequencies is achieved at 90Hz.

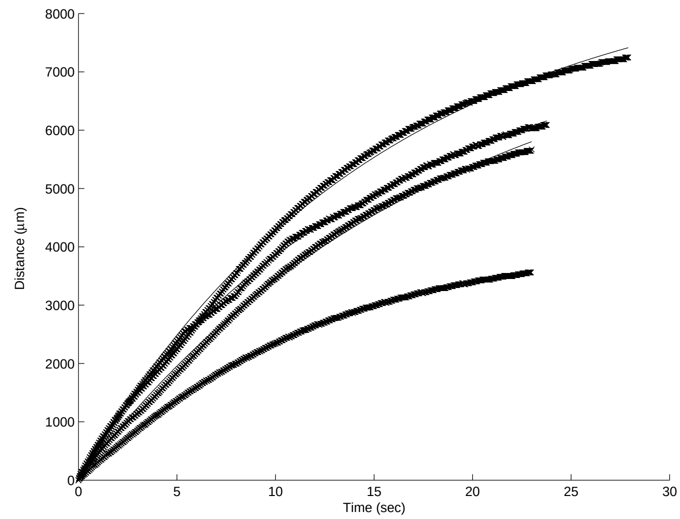

Figure 4. South motion translational displacements, plotted as “x”, and the best fit curve. Plots represent, from bottom up, 30, 60, 120, and 90Hz control frequencies. The highest velocity for these frequencies is achieved at 90Hz.

chips in opposing diagonals towards the center of mass of the robot. Using the robot’s directional and rotational control any angular orientation and translational position can be achieved.

The experiments consisted of running the microrobot for 25 seconds at an control frequency between 10Hz and 120Hz. An actuation voltage of 60V was used throughout the experiments. Each run was spaced 5 minutes apart to allow for the robot to cool to environmental temperatures. The northwest, south and counter clockwise motions were investigated for these experiments.

EXPERIMENTAL RESULTS

Displacement data results from the 30, 60, 90 and 120Hz iterations, plotted as “x”, with their respective best fit curves are shown in Figures 3, 4, 5.

The northwest motion travels almost 3 mm farther then the south in the same amount of time. This partially due to the thermal effects taking longer to set in because the actuators (in this case E-W) are not constantly powered as in the south motion.

The counter clockwise motion has less of an averaging effect then the other two investigated motions due to the two cilia chips pushing in opposite directions. This causes more noise to be present in counter clockwise motion.

Plots of the velocities calculated using the best fit curves are shown in Figures 6, 7, 8. The error bars in the graphs represent the error in approximating the displacement data with the best fit. The largest translational velocity of 635 μm/s is realized with the northwest motion at 110Hz.

For the lower frequency range, instantanious velocity increases as the control frequency is raised. Mechanical, frictional and to a lesser degree thermal limitations of the microactuators start to affect the chip movement at higher control frequencies. This is seen in the graphs by the more level velocities beyond 50Hz.

The south and counter clockwise motion exhibit similar patterns for the 10 to 60Hz range as a result of the chips being actuated with a non-diagonal motion in both cases.

At higher frequencies for the south and northwest movement, the pixel spacing size between the tracking circles in the video became smaller as a result of the larger frame of view necessary to capture the full 25 seconds of movement. With this smaller spacing comes pixel rounding errors that have a greater effect on the calculated displacement data and thus decreases the accuracy.

Wear

During testing of the microrobot each cilia has performed approximately 832k actuations with zero failures. This can be equated to a distance walked of 4.2 m with a step size of 5 μm. The only failures seen with the experimental setup is two control wires breaking when the robot is put away for the night. Previous related work has shown that cilia lifespan exceeds 20 million actuations per actuator with no actuation-related failures [26]. This equates to a distance traveled greater than 100 m.

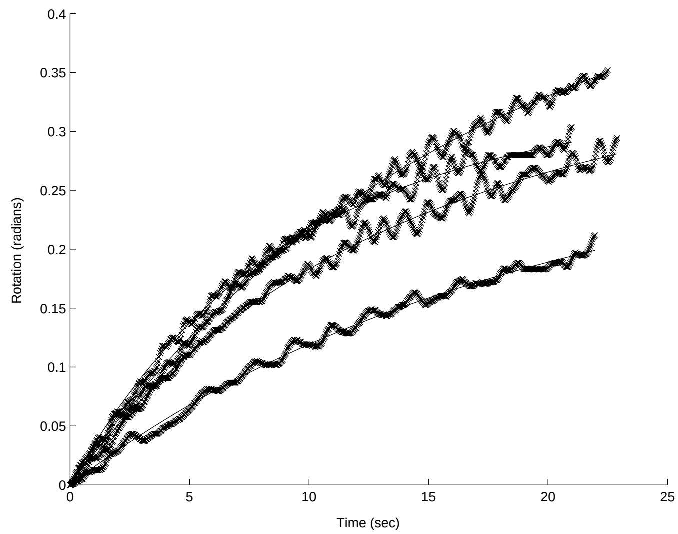

Figure 5. Counter clockwise rotational displacements, plotted as “x”, and the best fit curve. Plots represent, from bottom up, 30, 60, 90 and 120Hz control frequencies. The highest velocity for these frequencies is achieved at 120Hz.

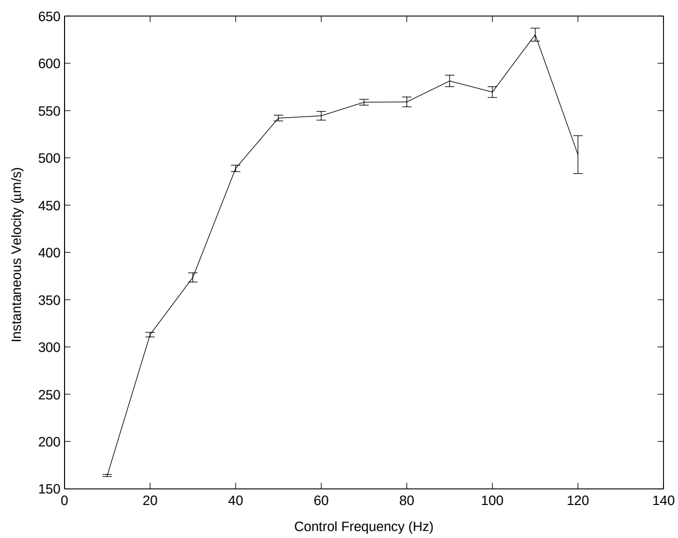

Figure 6. Northwest instantaneous velocity, calculated from best fit curve, versus the control frequency.

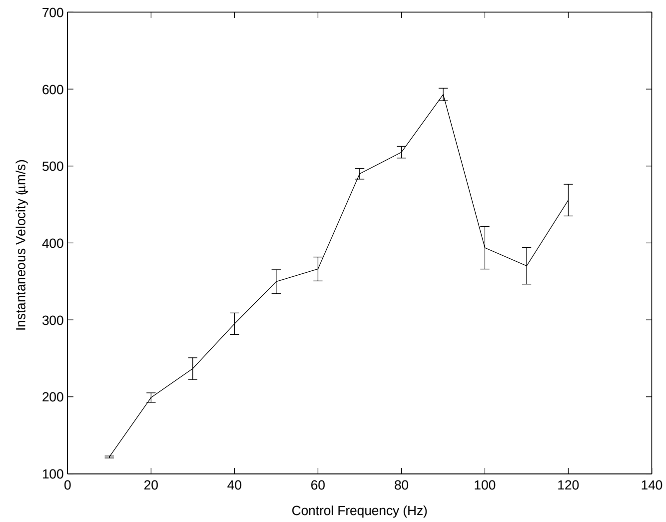

Figure 7. South instantaneous velocity, calculated from best fit curve, versus the control frequency.

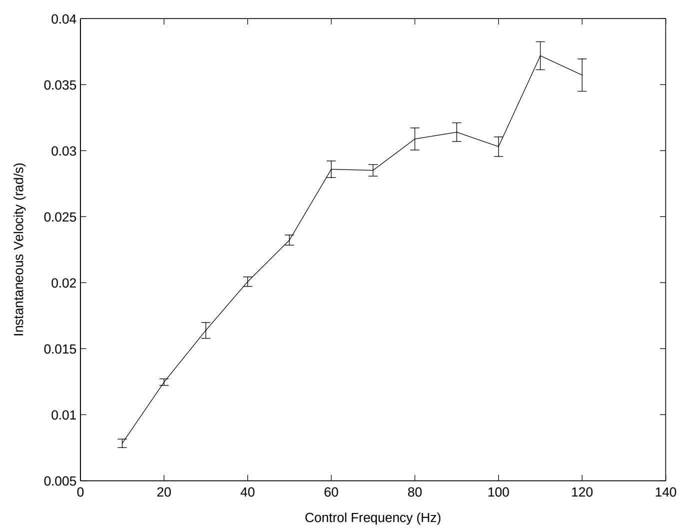

Figure 8. Counter clockwise instantaneous angular velocity, calculated from best fit curve, versus the control frequency.

CONCLUSION

The first MEMS walking microrobot to achieve reliable 3-DOF motion in the plane has been presented. Its performance has been extensively characterized and the results indicate that the thermal bimorph cilia arrays work well for microrobot locomotion. Motion in three degrees of freedom has been demonstrated and a maximum velocity of 635 μm/s and carrying capacity of greater than 1.448 g has been observed. In addition, the actuators have performed approximately 832,000 actuations, walking almost 4.2 m, with no failures. Our model (linear plus negative exponential) accurately describes the behavior of the microrobot.

Further investigation with this microrobot will include effects of heat build-up, surface properties and actuation voltage on the velocity and run-time.

ACKNOWLEDGMENT

This work was funded by NSF CAREER award ECS-9875367 (REU supplement) to K. Böhringer. The MEMS cilia controller was built with support from AFRL prime contract F29601-98-D-0210, USRA subcontract 9500-20. The MEMS cilia were built at the Stanford Nanofabrication Facility under support from DARPA contract N001-92-J-1940-P00001, a General Motors Key grant and NSF NYI award ECS-9358289-006 to G. Kovacs. The University of Washington MEMS lab acknowledges donations from Agilent Co., Intel Co., Microsoft Research, and Tanner Research Inc.

REFERENCES

[1] Fujita, H., 1993, "Group Work of Microactuators," *International Advanced Robot Program Workshop on Micromachine Technologies and Systems*, Tokyo, Japan, pp. 24–31.

[2] Böhringer, K.-F., Donald, B. R., Mihailovich, R., and MacDonald, N. C., 1994, "A Theory of Manipulation and Control for Microfabricated Actuator Arrays," *Proc. IEEE Workshop on Micro Electro Mechanical Systems (MEMS)*, Oiso, Japan, pp. 102–107.

[3] Böhringer, K.-F., Suh, J. W., Donald, B. R., and Kovacs, G. T. A., 1997, "Vector Fields for Task-level Distributed Manipulation: Experiments with Organic Micro Actuator Arrays," *Proc. IEEE Int. Conf. on Robotics and Automation (ICRA)*, Albuquerque, New Mexico, pp. 1779–1786.

[4] Böhringer, K.-F., Donald, B. R., and MacDonald, N. C., 1999, "Programmable Vector Fields for Distributed Manipulation, with Applications to MEMS Actuator Arrays and Vibratory Parts Feeders," Int. Journal of Robotics Research, pp. 168—200.

[5] Mita, Y., Kaiser, A., Stefanelli, B., Garda, P., Milgram, M., and Fujita, H., 1999, "A distributed microactuator conveyance system with integrated controller," *IEEE SMC '99*, vol. 1, pp. 18–21.

[6] Böhringer, K., and Choset, H., 2000, *Distributed Manipulation*, Kluwer Academic Publishers, Norwell, MA.

[7] Pister, K. S. J., Fearing, R., and Howe, R., 1990, "A Planar Air Levitated Electrostatic Actuator System," *Proc. IEEE Workshop on Micro Electro Mechanical Systems (MEMS)*, Napa Valley, California, pp. 67–71.

[8] Konishi, S., and Fujita, H., 1993, "A Conveyance System Using Air Flow Based on the Concept of Distributed Micro Motion Systems," *Transducers — Digest Int. Conf. on Solid-State Sensors and Actuators*, Pacifico, Yokohama, Japan, pp. 28–31.

[9] Mita, Y., Konishi, S., and Fujita, H., 1997, "Two Dimensional Micro Conveyance System with Through Holes for Electrical and Fluidic Interconnection," *Transducers — Digest Int. Conf. on Solid-State Sensors and Actuators*, Chicago, IL, vol. 1, pp. 37–40.

[10] Liu, C., Tsai, T., Tai, Y.-C., Liu, W., Will, P., and Ho, C.-M., 1995, "A Micromachined Permalloy Magnetic Actuator Array for Micro Robotics Assembly Systems," *Transducers — Digest Int. Conf. on Solid-State Sensors and Actuators*, Stockholm, Sweden, vol. 1, pp. 328–331.

[11] Liu, W., and Will, P., 1995, "Parts Manipulation on an Intelligent Motion Surface," *IEEE/RSJ Int. Workshop on Intelligent Robots & Systems (IROS)*, Pittsburgh, PA, vol. 3, pp. 399–404.

[12] Nakazawa, H., Watanabe, Y., and Morita, O., 1997, "The Two-Dimensional Micro Conveyor: Principles and Fabrication Process of The Actuator," *Transducers — Digest Int. Conf. on Solid-State Sensors and Actuators*, Chicago, IL, vol. 1, pp. 33–36.

[13] Furihata, T., Hirano, T., and Fujita, H., 1991, "Array-driven ultrasonic microactuators," *Transducers '91 Dig. 9th Int. Conf. on Solid-State Sensors and Actuators*, vol. 1, pp. 1056–1059.

[14] Böhringer, K.-F., Donald, B. R., and MacDonald, N. C., 1996, "Single-Crystal Silicon Actuator Arrays for Micro Manipulation Tasks," *Proc. IEEE Workshop on Micro Electro Mechanical Systems (MEMS)*, San Diego, CA, pp. 7–12.

[15] Takeshima, N., and Fujita, H., 1991, "Polyimide Bimorph Actuators for a Ciliary Motion System," *ASME WAM Symposium on Micromechanical Sensors, Actuators, and Systems*, vol. DSC-32, pp. 203–209.

[16] Ataka, M., Omodaka, A., and Fujita, H., 1993, "A Biomimetic Micro Motion System," *Transducers — Digest Int. Conf. on Solid-State Sensors and Actuators*, Pacifico, Yokohama, Japan, pp. 38–41.

[17] Suh, J. W., Glander, S. F., Darling, R. B., Storment, C. W., and Kovacs, G. T. A., 1996, "Combined Organic Thermal and Electrostatic Omnidirectional Ciliary Microactuator Array for Object Positioning and Inspection," *Proc. Solid State Sensor and Actuator Workshop*, Hilton Head, SC, pp. 168–173.

[18] Suh, J. W., Glander, S. F., Darling, R. B., Storment, C. W., and Kovacs, G. T. A., 1997, "Organic Thermal and Electrostatic Ciliary Microactuator Array for Object Manipulation," Sensors and Actuators A (Physical), **58**, pp. 51–60.

[19] Suh, J., Darling, R., Böhringer, K., Donald, B., Baltes, H., and Kovacs, G., 1999, "CMOS Integrated Ciliary Actuator Array as a General-Purpose Micromanipulation Tool for Small Objects," Journal of Microelectromechanical Systems, **8(4)**, pp. 483–496.

[20] Ebefors, T., Mattsson, J., Kälvesten, E., and Stemme, G., 1999, "A robust micro conveyor realized by arrayed poly-

imide joint actuators," *IEEE 12th Workshop on Micro Electro Mechanical Systems (MEMS)*, pp. 576–581.

[21] Kladitis, P., Bright, V., Harsh, K., and Lee, Y., 1999, "Prototype microrobotics for micro positiong in a manufacturing process and micro unmanned vehicles," *IEEE 12th Workshop on Micro Electro Mechanical Systems (MEMS)*, pp. 570–575.

[22] Ebefors, T., 2000, *Polyimide V-Groove Joints for Three-Dimensional Silicon Transducers*, Ph.D. thesis, Royal Institute of Technology, Stockholm, Sweden.

[23] Ebefors, T., Mattsson, J., Kälvesten, E., and Stemme, G., 1999, "A Walking Silicon Micro-Robot," *10th International Conference on Solid-State Sensors and Actuators*, pp. 1202–1205.

[24] Yeh, R., and Pister, K., 2000, "Design of Low-Power Articulated Microrobots," *International Conference on Robotics and Automation*, pp. 21–28.

[25] Darling, R., Suh, J., and Kovacs, G., 1998, "Ciliary microactuator array for scanning electron microscope positioning stage," Journal of Vacuum Science and Technology A, **16(3)**, pp. 1998–2002.

[26] Reiter, J., Terry, M., and Böhringer, K., 2000, "Thermobimorph microcilia arrays for small spacecraft docking," *ASME International Mechanical Engineering Congress and Exposition*.